J Neurophysiol 104: 2147–2157, 2010.
First published August 18, 2010; doi:10.1152/jn.00076.2010.

Neural Substrate of an Increase in Sensory Sampling Triggered by a Motor Command in a Gymnotid Fish

Virginia Comas and Michel Borde

Laboratorio de Neurofisiología Celular y Sináptica, Departmento de Fisiología, Facultad de Medicina, Universidad de la República, Montevideo, Uruguay

Submitted 19 January 2010; accepted in final form 16 August 2010

Comas V, Borde M. Neural substrate of an increase in sensory sampling triggered by a motor command in a gymnotid fish. *J Neurophysiol* 104: 2147–2157, 2010. First published August 18, 2010; doi:10.1152/jn.00076.2010. Despite recent advances that have elucidated the effects of collateral of motor commands on sensory processing structures, the neural mechanisms underlying the modulation of active sensory systems by internal motor-derived signals remains poorly understood. This study deals with the neural basis of the modulation of the motor component of an active sensory system triggered by a central motor command in a gymnotid fish. In *Gymnotus omarorum*, activation of Mauthner cells, a pair of reticulospinal neurons responsible for the initiation of escape responses in most teleosts, evokes an abrupt and prolonged increase in the rate of the electric organ discharge (EOD), the output signal of the electrogenic component of the active electrosensory system. We show here that prepacemaker neural structures (PPs) that control the discharge of the command nucleus for EODs are key elements of this modulation. Retrograde labeling combined with injections of glutamate at structures that contain labeled neurons showed that PPs are composed of a bilateral group of dispersed brain stem neurons that extend from the diencephalon to the caudal medulla. Blockade of discrete PPs regions during the Mauthner cell–initiated electrosensory modulation indicate that the long duration of this modulation relied on activation of diencephalic PPs, whereas its peak amplitude depended on the recruitment of medullary PPs. Temporal correlation of motor and sensory consequences of Mauthner cell activation suggests that the Mauthner cell–initiated enhancement of electrosensory sampling is involved in the selection of escape trajectory.

INTRODUCTION

Since the pioneering work of Sperry (1950) and von Holst and Mittelstaedt (1950), the idea of a modulation of sensory processing exerted by internal collaterals of motor signals has been commonly accepted. This kind of internal signals, known as corollary discharges (CD) or efference copies, has been widely implicated in the cancellation of self-generated sensory feedback during movement and other behaviors (McCloskey 1981). For example, in weakly electric mormyrid fishes, many mechanisms by which the motor command cancels the sensory feedback in hindbrain circuits have been elucidated (Bell 1989; Sawtell et al. 2005). The situation in the natural world, however, may require more complex interactions than simple cancellation (Crapse and Sommer 2008; Nelson and MacIver 2006; Poulet and Hedwig 2006; Sommer and Wurtz 2008). Indeed, motor commands may require increases or other modulations in active sensing as described, for example, in bats (Wilson and Moss 2004) and rats (Grant et al. 2009). These modulations could also be mediated by internal collaterals of motor commands, but these mechanisms have not been as widely studied.

The modulation of the electrogenic component of the active electrosensory neural system triggered by a motor command described in *Gymnotus omarorum*, a pulse-type gymnotiform fish (Falconi et al. 1995, 1997; Morales et al. 1993), emerged as a useful vertebrate model to analyze such high-level motor–sensory interactions. As in most weakly electric fish, the active electrosensory system in *G. omarorum* includes an electrogenic component, responsible for the emission of electric organ discharges (EODs), and an electroreceptive component devoted to the reception and processing of sensory signals evoked by their own self-generated electric fields during each EOD (Caputi 2004; Lorenzo et al. 2001). In this species, activation of the Mauthner cells (M-cell), the command neurons for escape responses in most teleosts, triggers an abrupt and prolonged increase in EOD rate [Mauthner-initiated abrupt increase in rate (M-AIR)]. Although motor activity could lead to an increase in EOD rate through a feedback sensory mechanism (Barrio et al. 1991; Lissman and Machin 1958), previous work indicates a neural connection between the Mauthner system and the electrogenic component of the active electrosensory system because M-AIR still occurs under pharmacological immobilization of the fish (Curti et al. 1999, 2006; Falconi et al. 1995, 1997). Moreover, the short latency of M-cell–triggered synaptic actions on pacemaker cells of the medullary pacemaker nucleus (PMn), the command nucleus for EODs (Curti et al. 2006; Falconi et al. 1997), points to a paucisynaptic neural pathway between both systems.

In most gymnotiform fish, modulations of EOD rate or waveform involve the activation of different prepacemaker structures (PPs) (Kawasaki et al. 1988; Keller et al. 1991). These structures may function as neural centers at which several processed inputs are subsequently transformed into specific modulations of the activity of the PMn (Caputi et al. 2005; Keller et al. 1990; Lorenzo et al. 2001; Santana et al. 2001). We hypothesize that, in *G. omarorum*, PPs are also involved in the organization of the M-cell–initiated enhancement of electrosensory sampling. To test this hypothesis, PPs were first identified according to anatomical and functional criteria and effects of their specific blockade on M-AIR were assessed. Our data indicate that a set of functionally segregated PPs are key elements of this modulation and suggest that an enhancement of electrosensory sampling triggered by M-cell activation is involved in motor sequencing during escape.

Address for reprint requests and other correspondence: M. Borde, Dpto. de Fisiología, Facultad de Medicina. Gral. FLORES 2125, CP 11800, Montevideo, Uruguay (E-mail: mborde@fmed.edu.uy).

METHODS

Fifty-five juvenile specimens of *G. omarorum* nov. sp. (formerly identified as *Gymnotus carapo*; Richer-de-Forges et al. 2009) with a mean length of 16 ± 2.8 (SD) cm were used in this study. All experimental procedures were previously described in detail (Falconi et al. 1995); they were conducted in accordance with the guidelines set forth by the Comisión Honoraria de Experimentación Animal, Universidad de la República ("Uso de animales en experimentación, docencia e investigación Universitaria," CDC Exp. 4332/99, Diario Oficial 25467, Feb. 21/00).

Surgical procedures

Fish were anesthetized by immersion in iced water. All surgical areas and fixation points were infiltrated with lidocaine. During surgical procedures, the gills were perfused with aerated iced tap water. The paravertebral muscles were removed from one side of the fish at the caudal portion of the tail (at ~80% of the fish length) to place a bipolar stimulating electrode in contact with the vertebral column. Electrical stimuli were applied to the spinal cord using this electrode to determine the threshold intensity required to induce the tail flip that follows M-axon activation. The dorsal surface of the brain was exposed through an opening in the skull to provide access for micropipettes used for recording and drug application at different deep brain stem structures. Following these procedures, the animals were injected with d-tubocurarine (1–3 μg/g, im) at doses that produced paralysis but did not completely eliminate the EOD. After surgical preparation and curarization, the gills were continuously perfused with aerated tap water at room temperature (20–25°C).

Recording and stimulation procedures

In most experiments, the same micropipette was used for field potential recordings and drug application. Electrical recordings were obtained using micropipettes filled with NaCl (154 mM)-based solutions of different compounds connected to an Axoclamp 2B amplifier (Axon Instruments, Foster City, CA). A Grass Technologies (Quincy, MA) P15 preamplifier was used to monitor the EOD (head to tail) with a pair of metal electrodes placed next to the fish and in contact with the supporting wet sponge, with a gain of 100× and low-pass filtered (cut-off at 3 KHz). The signals were displayed on an oscilloscope and stored on magnetic tape. Data acquisition and analyses were performed using a Macintosh CI microcomputer (Apple Computers, Cupertino, CA) using specially designed software. Superscope software (GW Instruments, Somerville, MA) was used to construct instantaneous frequency versus time plots.

Retrograde labeling experiments

Micropipettes were filled with a 2% solution of biocytin (Vector Laboratories, Burlingame, CA) in 0.5 M KCl and were used for recording and cell marker application. Guided by the characteristic waveform of the PMn field potential (Curti et al. 2006) (Fig. 1*B*), biocytin was iontophoresed near pacemaker cells (PM-cells) using a PSIU6 isolation unit (Grass Technologies) delivering 500 ms pulses of 2–6 μA, with alternate polarities at 0.5 Hz for 30–60 min. After biocytin iontophoresis, the skull was sealed with gelfoam and dental acrylic, and the animal was allowed to survive for 2–5 days (Kawasaki et al. 1988). Animals were deeply anesthetized by immersion in iced water; the brains were removed and fixed overnight by immersion in paraformaldehyde (4%). Once embedded in gelatin (5% in 0.9% NaCl solution), the brains were mounted in a Vibroslicer (Campden, Lafayette, IN) and serially sliced (80 μm) at transverse or horizontal planes. Biocytin-labeled cells were visualized using the Vectastain ABC System (Vector Laboratories, Burlingame, CA), based on standard procedures as described by Horikawa and Armstrong (1988). Brain

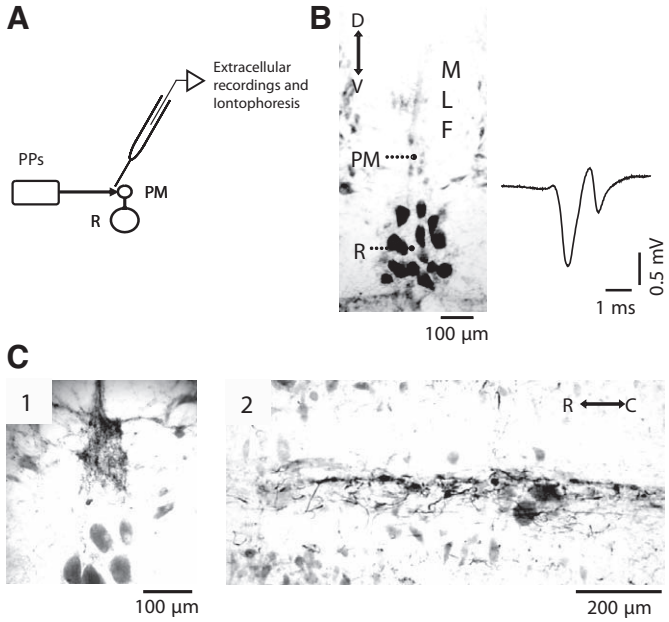

FIG. 1. *A*: schematics of the experimental design for retrograde labeling of prepacemaker structures (PPs) showing the pacemaker nucleus (PMn) composed by pacemaker (PM) and relay (R) cells innervated by PPs and the micropipette used for both extracellular recording and dye iontophoresis. *B*: photomicrograph of the PMn (*left*) of a representative transversal section approximately through the center of the nucleus depicting the localization of PM and R cells. MLF, medial longitudinal fasciculus. Biocytin was iontophoresed in the vicinity of PM-cells; location is indicated by the presence of a typical field potential recording (*right*). *C*: photomicrographs of representative transversal (*1*) and horizontal (*2*) sections showing the distribution of tracer deposits at the injection site within the PMn. Note that the dye distributed almost exclusively at the level of PM-cells.

sections were counterstained with Pyronin-Y red, mounted, and examined with a Nikon Optiphot microscope. Digital photographs were taken with a Kodak MDS120 camera. Labeled cells were counted by two independent observers in every case, and only neurons whose somata were unequivocally labeled were included in the counts. Despite probable minor species-specific differences, nuclei and structures referred to in the description of anatomical data were defined in accord to the stereotaxic atlas of *Apteronotus*, a wave-type weakly electric fish (Maler et al. 1991).

Exploration of Glu sensitivity

At brain stem locations selected according to the distribution of labeled cells, microdroplets (10–30 μm diam measured in air) of a glutamate solution (Glu, L-glutamic acid 10 mM, dissolved in 154 mM NaCl) were applied by pressure (10–40 psi, 50–60 ms) at discrete locations, 100 μm apart, during exploratory vertical tracks using a Picospritzer II injector (General Valve, Fairfield, NJ). EOD rate and waveform were monitored before, during, and after each Glu ejection. At a given region, a series of ≥10 exploratory vertical tracks of 1,500 μm were performed at two or three different distances from midline (range from 400 to 900 μm) and at four or five positions in the rostrocaudal axis. Although exploration of Glu sensitivity was centered in the depth range at which labeled neurons were observed, in most experiments, vertical tracks also explored more superficial and ventral regions. For each vertical exploratory tract, depth series of EOD rate modulations evoked by Glu at each ejection site were constructed. Responses were considered short latency when the first EOD interval affected by Glu ejection coincided with the interval at which ejection occurred.

Activation of Mauthner cells

M-cells axons were stimulated at the spinal cord with rectangular current pulses (0.15–0.3 mA, 0.2–0.5 ms), which were sufficient to activate both M-cell axons. This was determined by the amplitude of M-AIR (Falconi et al. 1995) and confirmed during extracellular recordings from the left M-cell by the appearance of the characteristic sequence of electrical events produced by the activation of one or both M-cell axons (Borde et al. 1991). In most experiments, M-cells were activated by single stimuli repeated at a low rate (every 3 min). For the experiments that were designed to study the role of medullary PPs in M-AIR, M-cells were also activated by paired, conditioning test stimuli with an interval of 8 s. This protocol was used to reduce synaptic efficacy at M-cell output synapses (Curti et al. 2006; Waldeck et al. 2000) and thus to decrease the M-cell–dependent excitatory drive to prepacemaker neurons in responses evoked by the test stimulus of each pair. Under these conditions, local application of relatively small volumes of blocker solutions will prevent the recruitment of a comparatively larger population of medullary prepacemaker cells during M-AIR. Paired M-cell stimuli were applied at regular intervals (3 min) before and after specific blockade of PPs.

Lesion and pharmacological blockade experiments

To exclude diencephalic PPs from the putative neural circuit responsible for organizing the M-AIR (see Fig. 7*B*), we carried out a complete brain stem transection at the caudal limit of the tectum using a dissecting scalpel blade. In addition, for transient blockade of restricted portions of PPs, glutamate antagonists (±)-2-amino-5-phosphonopentanoic acid (AP5, 500 μM) combined with 6-cyano-7-nitroquinoxaline-2,3-dione2-hydroxypropyl-cyclodextrin-complex (CNQX, 500 μM), dissolved in NaCl (154 mM), were pressure ejected (30 psi, 50–300 ms), usually unilaterally, into the diencephalon, the octavolateral area, and within the caudal medulla. In these experiments, approximate coordinates in the rostrocaudal, lateral, and vertical directions of sites of maximal EOD responses to Glu application were first determined; thereafter, microdroplets of antagonist solutions of ~100 μm diam (measured in air) were applied at these locations. In some experiments, the possibility of unwanted diffusion of blockers onto the PPs-pacemaker cells synapse was assessed by monitoring EOD accelerations elicited by local Glu pressure application (10–20 psi, 50–100 ms) in the vicinity of PM-cells. Glutamate, AP5, and CNQX were obtained from Sigma-Aldrich (St. Louis, MO).

The peak amplitude of M-AIR was measured before and after surgical or pharmacological blockade of PPs. In addition, because the full duration of M-AIR may be indirectly affected by changes in M-AIR amplitude, we calculated the decay time constant (τ_{DEC}) of the response. For this purpose, M-AIR decay phase was fitted with a single exponential function using Clampfit routines of PClamp 8.0 software (Axon Instruments, Foster City, CA). Changes in both peak amplitude and τ_{DEC} were expressed as percentage of controls.

Statistical analysis

For assessing the statistical significance of changes produced by drug- or lesion-induced conditions, the two-tailed paired Student *t*-test was used. Unless otherwise indicated, summary data are expressed as mean ± SD.

RESULTS

Identification of PPs

In this study, the term prepacemaker is applied to specific neuronal populations that project directly on the PMn *and* modulate the activity of PMn and hence of EODs. Accordingly, our first series of experiments was aimed at identifying putative PPs through both morphological and functional criteria.

Retrograde tracing experiments

Previous work indicates that PM-cells are the exclusive cellular target for glutamatergic afferents involved in M-AIR (Curti et al. 1999, 2006). Accordingly, biocytin was iontophoresed at the PMn where PM-cells are located in eight animals. The micropipette filled with biocytin solution was used for both extracellular recording and iontophoresis (Fig. 1*A*). The exact location of the biocytin-filled micropipette relative to the different cell types that comprise the PMn was assessed by the waveform of the field potential produced by the spontaneous pacemaker activity. This field potential is phase-locked with and precedes each EOD (Curti et al. 2006). In *G. omarorum*, pacemaker and relay cells are spatially segregated within the PMn; whereas PM-cells concentrate within the dorsal aspects of the nucleus, relay cells occupy its ventral portion (Fig. 1*B, left*). In the vicinity of PM-cells, near the center of the nucleus in the rostro-caudal axis, field potentials elicited by pacemaker activity are characterized by two successive negative-going waves with specific amplitudes and time courses (Fig. 1*B, right*) (Curti et al. 2006). Examination of the injection sites invariably showed that the marker was present almost exclusively within the location of PM-cells (Fig. 1C_1). Although biocytin was iontophoresed near the rostro-caudal center of the PMn, extracellular deposits of the marker and several labeled PM-cells somas were consistently observed throughout the rostro-caudal extent of the nucleus (Fig. 1C_2).

The number of labeled neurons per animal was relatively small (mean = 33, range = 7–158) and was systematically observed at the diencephalon, the octavolateral area, and the caudal medulla. Representative examples are shown in Fig. 2. At the diencephalic level (Fig. 2*A*), labeled neurons were located in a region that lies ventrolaterally to the nucleus centralis posterior (CP) of the thalamus and laterally to the periventricular nucleus of the posterior tuberculum (nTPP). The shape and diameter of the somas and the appearance of their dendritic arbors varied considerably. Although most labeled cells (≤80%) exhibited small ovoid somas (mean diameter, 11.6 ± 3.6 μm), a few multipolar cells with larger somas (mean diameter, 19.3 ± 1.0 μm) were also consistently observed. Ovoid and multipolar cells appeared intermingled without an apparent topographical organization.

In the octavolateral area, a region located laterally and dorsally to the M-cell somas (Fig. 2*B*), labeled neurons were observed in the medial aspects of the medial octavolateral nucleus (MON). In this region, most of the labeled cells exhibited relatively large somas (mean diameter, 17.8 ± 3.3 μm) and dendritic arbors that extended mainly in a ventral and lateral direction, toward the magnocellular octavolateral nucleus.

Labeled neurons in the caudal medulla were distributed along a bilateral rostro-caudal column located in an intermediate zone lateral to the medial longitudinal fasciculus at the dorsal limits of the reticular formation (Fig. 2*C*). Their somas were moderately elongated (mean diameter, 19.6 ± 4.6 μm) and exhibited thin dendrites that projected in a dorsal and lateral direction.

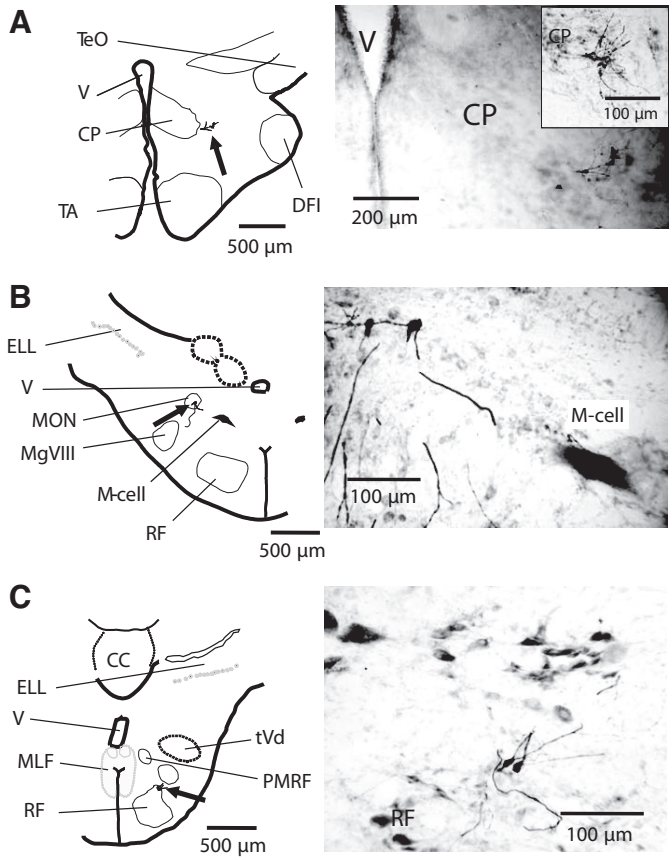

FIG. 2. Camera lucida drawings (*left*) and photomicrographs (*right*) of representative transverse sections through the diencephalon (*A*), the rostral medulla at the level of M-cells (*B*), and at the caudal medulla (*C*), showing the distribution of retrogradely labeled cells after byocitin deposits near PM-cells at the PMn. *A*: at the diencephalon, labeled cells appeared in the vicinity of the central posterior (CP) thalamic nucleus (*left*, oblique arrow). *Inset*: a photomicrograph at higher magnification obtained from a horizontal section showing a group of labeled cells bodies and several dendritic branches extending rostrolaterally and caudolaterally. *B*: at the octavolateral area, marked neurons distributed in a region lateral and dorsal to the M-cells, within or in the close proximity of the medial octavolateral nucleus (*left*, oblique arrows). The cell body of the M-cell is evident in the photomicrograph at *right*. *C*: in this representative transversal section obtained at ~1,000 μm from the PMn in the rostral direction, retrograde labeled cells appeared at the dorsal limit of the reticular formation (*left*, oblique arrow). CC, crista cerebellaris; CP, central-posterior nucleus; DFl, nucleus diffusus lateralis of the inferior lobe; ELL, electrosensory lateral line lobe; M-cell, Mauthner cell; MgVIII, magnocellular octavolateral nucleus; MLF, medial longitudinal fasciculus; MON, medial octavolateral nucleus; PMRF, paramedian reticular formation; RF, reticular formation; TA, nucleus tuberis anterior; TeO, optic tectum; tVd, descending trigeminal tract; V, ventricle.

Results from retrograde tracing experiments are summarized in Fig. 3. In the rostro-caudal axis, labeled cells were distributed unevenly along a bilateral column that extended from the diencephalon, in the proximity of the CP of the thalamus, to an area located near the rostral pole of the PMn (Fig. 3*A*). In the frontal plane, the location of labeled neurons observed in all animals ($n = 6$) is shown by the shaded areas in three representative transversal sections (Fig. 3, *B–D*). Marked neurons in close association with the CP of the thalamus (Fig. 3*B*) most likely encompass the diencephalic prepacemaker nucleus that has been described in most gymnotiform fish (Heiligenberg et al. 1981; Kawasaki et al. 1988; Keller et al. 1991; Kennedy and Heiligenberg 1994). In contrast, labeled neurons located at the octavolateral area, in the vicinity of M-cell somas (Fig. 3*C*), and at the caudal medulla (Fig. 3*D*) were not included in previous descriptions of prepacemaker neurons in gymnotiform fish (ibid).

In three of six animals, few labeled neurons (in total 18) were also present in a brain stem region ~1,000 μm rostral to M-cells, lateral to the locus coeruleus and the subcoeruleus nucleus, and ventral to the paralemniscal nucleus near the dorsal boundaries of the mesencephalic reticular formation (data not shown).

Activation of putative PPs by glutamate

The anatomical evidence obtained by retrograde labeling after biocytin injection into the PMn strongly suggests that several neuronal groups control the activity of this nucleus in *G. omarorum*. However, to be postulated as PPs, the activation of these neuronal groups must induce evident short-latency modulations of PMn discharge that are usually detected as changes in the frequency or waveform of EODs (Juranek and Metzner 1998; Kawasaki and Heiligenberg 1990). Therefore to verify whether the populations of neurons that were retrogradely labeled in the diencephalon, octavolateral area, and

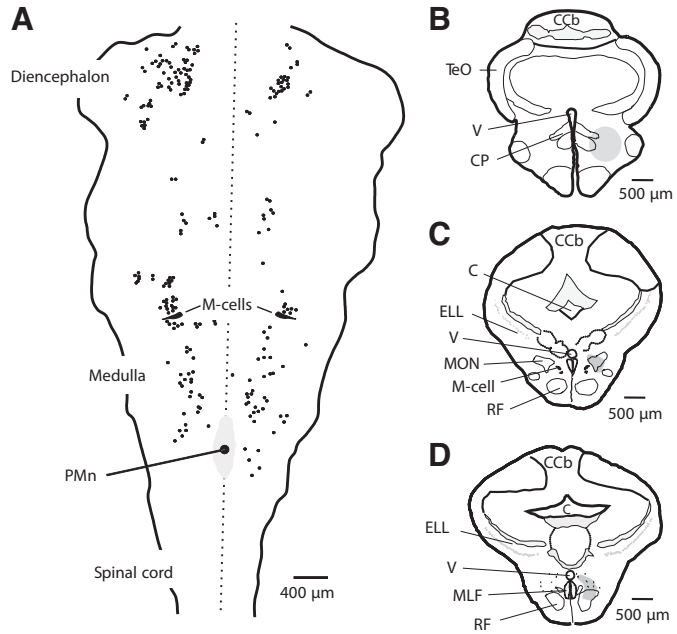

FIG. 3. Summary of retrograde labeling in the diencephalon and brain stem after tracer deposits in the vicinity of PM cells at the pacemaker nucleus. *A*: most of labeled cells somas (black dots) observed in our successful retrograde labeling experiments (6 of 8 animals) were included in a schematic of a representative horizontal section that comprises the diencephalon, the brain stem, and the rostral spinal cord. The M-cell bodies and the PMn, 2 neural structures that were taken as references in our study, are also shown. The midline is represented by a dotted vertical line. *B–D*: rostral to caudal series of camera lucida drawings of representative transversal sections through the diencephalon, the octavolateral area, and the caudal medulla, 3 specific levels of the neuraxis selected for analysis. At each level, the shaded area (dark gray at ventral right quadrant) represents a hypothetical surface that contains most of labeled neurons observed in 6 animals. Representative section at the caudal medulla corresponds to a region approximately halfway between the PMn and the M-cells. C, cerebello-medullary cistern; CCb, corpus cerebelli; CP, central-posterior nucleus; ELL, electrosensory lateral line lobe; M-cell, Mauthner cell; MLF, medial longitudinal fasciculus; MON, medial octavolateral nucleus; RF, reticular formation; TeO, optic tectum; V, ventricle.

caudal medulla play a PP role, we carried out local microinjections of glutamate in these regions in conjunction with EOD recording.

Representative examples of maximal responses evoked by Glu ejection within the three regions explored are shown in Fig. 4. Along a vertical track located 650 μm laterally to the midline at the diencephalon, the maximal response was observed at a depth of 2,600 μm and consisted of a short-latency increase in EOD rate ($\leq$6 Hz) that lasted $\geq$2.5 s (Fig. 4*A1*). From this site, the amplitude of the response decreased to a 37% of the maximum response at a level located 600 μm dorsally and almost disappeared at a location situated 200 μm ventrally (Fig. 4*A2*). Systematic exploration of Glu sensitivity at this region in seven animals showed that maximal responses were observed at a mean depth of 2,800 $\pm$ 160 μm from the brain surface. In all cases, Glu provoked increases in EOD rate without changes in EOD waveform. In Fig. 4*A3*, sites of maximal responses observed in these experiments (black dots) are depicted in a diencephalic coronal section according to their lateral and vertical coordinates. Maximal Glu-responsive sites overlap with the region of labeled neurons observed at the diencephalon near the thalamic CP (see Fig. 3*B*). In three animals Glu sensitivity was also explored at more dorsal locations along vertical tracks (see *inset* in Fig. 4*A3* for a representative example). Another region at which Glu ejection evokes significant increases in EOD rate ($\leq$80% from maximum although with a slower time rise) was detected at a depth range of 1,700–2,100 μm from the surface of the brain (gray spots in Fig. 4*A3*). Responses produced by Glu ejection within this region most likely resulted from activation of neural elements encompassing the medial region of the torus semicircularis ventralis.

Systematic exploration of Glu sensitivity at the octavolateral area was facilitated because the M-cells, which can be easily recognized electrophysiologically (Borde et al. 1991; Faber and Korn 1978; Furshpan and Furukawa 1962), served as a topographical reference in this region of the brain stem. The tip of a Glu pipette, also used to perform extracellular recordings, can be placed deeply in the brain stem at known distances from the M-cell axon cap (Furshpan and Furukawa 1962). Along the vertical track that evoked the maximal response, Glu ejection at a depth of 2,900 μm (~800 μm from midline and 350 μm lateral to M-cell axon cap) produced a short-latency increase in EOD rate of ~8.6 Hz that lasted for 4.9 s (Fig. 4*B1*). Along the same track, responses were almost absent 300 μm dorsally, decreased gradually (although nonmonotonically) toward more ventral ejection sites, and vanished at 700 μm from the site of maximal response (Fig. 4*B2*). In 16 animals, maximal responses were observed at a mean depth of 2,750 $\pm$ 420 μm. Sites of maximal responses observed in these experiments are depicted in a typical coronal section at the level of the M-cells (Fig. 4*B3*, black dots) according to their lateral and vertical coordinates respect to the M-cell. These sites encompass the octavolateral area, i.e., the same region where biocytin retrogradely labeled neurons were present (see Fig. 3*C* for comparison). In six animals, exploration of Glu sensitivity including more dorsal regions also showed responses to Glu ejection ($\leq$75% of maximum, although with a slower time course), in a depth range of 1,500–2,200 μm (gray dots, Fig. 4*B3*); a representative example is shown in the *inset* in Fig. 4*B3*. Responses that followed glutamate application at these more dorsal sites most likely resulted from activation of medial portions of the electrosensory lateral line lobe (ELL).

At the caudal medulla, exploration of Glu sensitivity was carried out at three different rostro-caudal levels separated by 500 μm, with similar overall results. The tip of the Glu pipette was positioned rostrally to the PMn, which served as reference. Figure 4*C* shows results obtained from a vertical track conducted 500 μm from midline and ~1,000 μm rostral to the center of the PMn. At a depth of 2,800 μm (Fig. 4*C1*), Glu

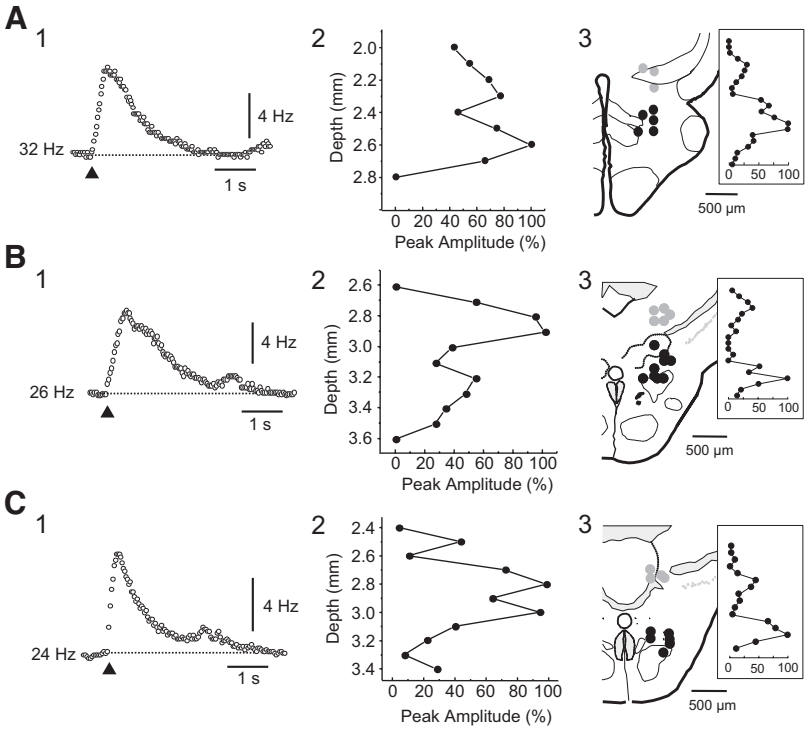

FIG. 4. Electric organ discharge (EOD) modulations produced by activation of PPs by local glutamate pressure ejection. *A*: exploration of Glu sensitivity at the diencephalon. *1*: plot of EOD frequency vs. time of an example of maximal EOD rate response to Glu (10 mM, 20 ms, 15 psi) during a vertical exploratory tract performed at 650 μm from midline. *2*: depth profile of EOD rate responses during the same vertical tract. *3*: sites of maximal Glu sensitivity observed during these experiments are shown (black dots) in a quadrant of a schematic drawing of a representative transversal section. Sites of Glu sensitivity identified at more dorsal locations (gray dots) are also represented. *Inset*: illustrative depth profile of responses to Glu (% of peak amplitude) during an extended exploratory vertical tract (from 1.5 to 3.6 mm). Depth axis, same scale as part 3. *B* and *C*: same structure as in *A* but during exploration of Glu sensitivity at the octavolateral area and at the caudal medulla respectively. Depth ranges explored were 1.4–3.3 and 1.6–3.1 mm for *insets* in *B* and *C*, respectively. For all EOD frequency vs. time plots, the moment of Glu ejection is indicated by the arrowhead, and the dotted line shows basal EOD frequency indicated in each trace by the numbers at *left*.

ejection provoked a short-latency increase in EOD rate of 7.9 Hz that lasted for 3.7 s. Along this vertical track, amplitude of responses decreased nonmonotonically in both dorsal and ventral directions and was virtually absent at a distance of 400 μm from the most effective depth (Fig. 4*C2*). Overall, sites of maximally induced EOD responses after Glu application within the caudal medulla (6 animals, ≤36 vertical tracks) were located at a mean depth of 2,810 ± 90 μm. Ejection sites that elicited maximal responses are shown in a representative coronal section (black dots, Fig. 4*C3*). The area of Glu sensitivity in the caudal medulla approximately corresponds to the region of labeled neurons (see Fig. 3*D* for comparison). Vertical tracks that explored more rostral levels within the caudal medulla ($n = 4$) detected an additional area of Glu sensitivity at a depth range of 1,700–2,100 μm (gray dots, Fig. 4*C3*), which most likely result from activation of the nucleus medialis. An illustrative depth profile including dorsal and ventral Glu-sensitive areas is depicted in the *inset* in Fig. 4*C3*.

Structures activated by injections of Glu at relatively dorsal locations in the diencephalon, the octavolateral area, and the caudal medulla are likely involved in the processing of sensory information from different sources (i.e., ventral torus, ELL, nucleus medialis). Thus their activation by Glu may evoke EOD rate modulations similar to those observed during sensory-evoked novelty responses.

Role of PPs in M-AIR

The M-cell–initiated modulation of the active electrosensory neural system consists of an abrupt and short latency acceleration of EODs (≤40% increase in rate), which is long-lasting (≥1 s) (Curti et al. 2006; Falconi et al. 1997). Its short delay (~4 ms for synaptic actions at PM-cells) indicates that the pathway between Mauthner and PM-cells includes only a few interposed neuronal structures. One way to investigate in vivo the role of PPs in this modulation includes the analysis of M-AIR changes produced by a complete exclusion of PPs from the underlying neural circuit. However, the fact that in *G. omarorum* PPs are likely represented by a widely distributed bilateral group of neurons extending from the diencephalon to the caudal medulla precludes any attempt to carry out this kind of experiment. Consequently, the role of selected sectors of PPs in M-AIR was assessed by means of two different technical approaches: *1*) the exclusion of more rostral PPs by brain stem transection at the level of the caudal limit of the tectum and *2*) the transient blockade of restricted portions of PPs (diencephalic region, octavolateral area, and caudal medulla) by local application of ionotropic glutamate receptor antagonists. Before surgical or pharmacological blockade of PPs, M-AIRs were as previously described, exhibiting mean peak amplitude of 9.7 ± 4.4 Hz ($n = 43$), mean total duration of 2.9 ± 1.3 s ($n = 43$), and mean τ_{DEC} of 0.67 ± 0.40 s ($n = 43$).

Diencephalic PPs

According to the putative neural circuit that controls M-AIR (see Fig. 7*B*), the contribution of most rostral PPs to M-AIR, i.e., diencephalic PPs, is expected to be eliminated by a complete transversal section of the brain stem at the caudal limit of the tectum (see Fig. 5*A* for a scheme). Accordingly, M-AIR was examined before and after brain stem transection in nine animals.

EOD frequency usually increased (7–10 Hz) immediately after transection, returned to control values in ~2 min, and remained stable for the remaining of the experiment (≤90 min). Modifications of M-AIR were evaluated after complete recovery of EOD basal frequency. As shown in Fig. 5*B*, the peak amplitude of M-AIR was reduced to 91.4% of control (from 7.7 to 6.8 Hz) by brain stem transection, whereas the duration of the response decreased from 2.3 to 0.97 s, with a reduction of τ_{DEC} to 36.6% of control. These changes persisted for the remaining of the experiment (i.e.: 90 min). Similar results, although reversible, were obtained by bilateral local application of CNQX-AP5 solutions at the level of diencephalic PPs (11 injections, 7 animals). As shown in Fig. 5*C*, after bilateral injections of glutamate antagonists (100 ms, 30 psi) into the region of diencephalic PPs, M-AIR shortened, with a decrease of τ_{DEC} to 33.4% of control, whereas peak

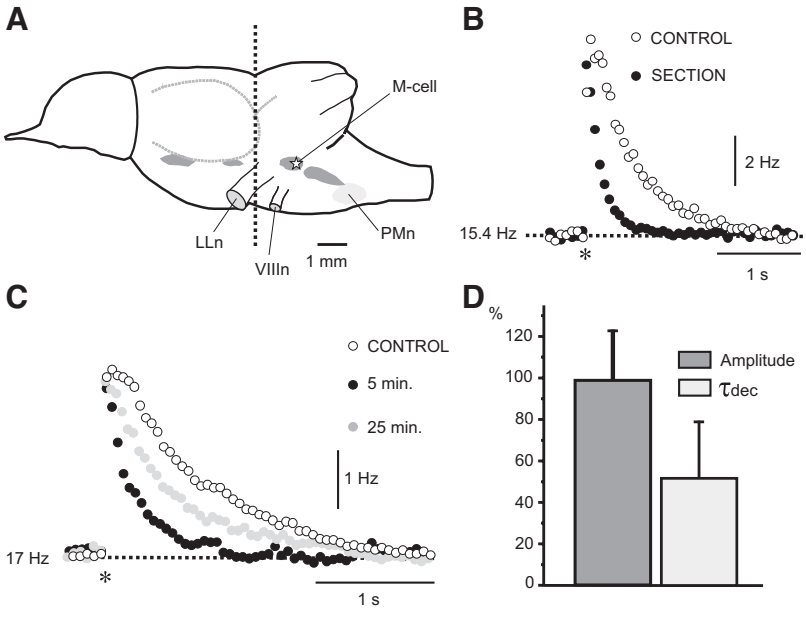

FIG. 5. Recruitment of diencephalic PPs determines the duration of Mauthner-initiated abrupt increase in rate (M-AIR). *A*: schematic drawing of a lateral view of the brain of *Gymnotus omarorum*. Lateral line (LLn) and VIII nerves (VIIIn) are also depicted. The approximate location of M-cells and of the PMn was included in the scheme for reference. The vertical dotted line indicate the level at which the brain stem was sectioned during the analysis of the role of diencephalic PPs in M-AIR. Dark gray areas represent the most prominent groups of retrogradely labeled neurons whose activation by Glu evoke short-latency EOD accelerations. *B*: plots of EOD frequency vs. time of single M-AIRs evoked before (○, CONTROL) and 3 min (●, SECTION) after the complete brain stem section at the level indicated in *A*. *C*: plots of EOD frequency vs. time of single M-AIRs evoked before (○, CONTROL) and 5 (●) and 25 min (●) after bilateral pressure ejection of a solution of glutamate antagonists (AP5 500 μM and CNQX 500 μM in NaCl 154 mM, 30 psi, 100 ms) at diencephalic PPs. In *B* and *C*, the moment of M-cell activation at the spinal cord is indicated by an asterisk, and the dashed line shows basal EOD frequency indicated in each trace by the numbers at *left*. *D*: summary data (mean ± SD, $n = 20$) of effects of diencephalic PPs blockade on M-AIR amplitude (dark gray bar) and decay time constant (τ_{DEC}, light gray bar) plotted as percentages of their respective control values.

amplitude showed a reduction to 91.6% of control. These effects slowly reversed, and M-AIR recovered control parameters in ~75 min (range, 50–90 min) after injections. Results from brain stem transection and from CNQX-AP5 bilateral application at diencephalic PPs are summarized in Fig. 5*D* ($n = 20$). Blockade of diencephalic PPs produced a marked reduction of the duration of M-AIR with a decrease of τ_{DEC} to a mean value of 52.1 ± 28.1% of control, with minor effects on its peak amplitude (mean peak amplitude after blockade, 99.1 ± 25.1% of control). Whereas changes in M-AIR τ_{DEC} reached statistical significance ($P = 0.0013$), those observed in peak amplitude did not ($P = 0.4$).

Medullary PPs

Because of their scattered distribution along an extended area between the PMn and the vicinity of M-cells, the role of medullary PPs on M-AIR was studied only by local application of CNQX-AP5 solution at the octavolateral area and at two discrete regions located at known distances (500 and 1,000 μm) from the PMn in the rostral direction and at 500–600 μm from midline.

In a first series of experiments (7 animals), M-AIR was evoked at regular intervals (typically 3 min), and its peak amplitude and duration were monitored before and after a single injection of Glu antagonists at a given location. From a total of 29 injections, minimal reversible changes in M-AIR were observed only in 4 injections (13.8%). In these cases, M-AIR peak amplitude (but not duration or τ_{DEC}) was slightly reduced to 92.2 ± 9.3% of controls ($P = 0.003$). The lack of effect following most of Glu antagonist injections (86.2%) may have been because of the possibility that the number of PPs neurons effectively blocked was not sufficiently large to produce evident effects on M-AIR. As described for most M-cell output pathways (Faber et al. 1989), PPs neurons may be activated by synapses with a high efficacy and probably are part of a highly redundant pathway. In line with this assumption, and considering that activation of M-cell associated circuits is reduced by repetitive M-cell activation (Curti et al. 2006; Faber et al. 1989; Waldeck et al. 2000), the effect of injections of Glu blockers at medullary PPs on M-AIR was re-examined (21 animals) using repetitive M-cell stimulation to reduce synaptic efficacy at M-cell output pathways. Instead of using prolonged repetitive M-cell stimulation that produces a marked suppression of M-AIR (Curti et al. 2006), we designed a stimulation protocol directed to moderately reduce synaptic efficacy at M-cell output pathways without significantly affecting either M-AIR peak amplitude or duration. This was achieved by using paired, conditioning test stimulation of M-cells with an interval of 8 s. This was confirmed in selected experiments ($n = 4$) by simultaneously recording the M-AIR and the so-called "extrinsic hyperpolarizing potential" (EHP), an electrical event that reflects synchronous activation (burst of action potentials) of a population of recurrent inhibitory interneurons (Borde et al. 1991; Charpier et al. 1994; Faber and Korn 1978; Furukawa and Furshpan 1963). Paired M-cell activation reduced synaptic efficacy at the recurrent inhibitory circuit (Fig. 6*A*, EHP, *bottom panel*), as indicated by a slight increase in the latency of EHP (108.3 ± 4.1%, $P = 0.145$) and a reduction of its amplitude (3rd peak decreased to 77.9 ± 5.7% of control, $P = 0.038$), whereas M-AIRs produced by both conditioning and test stimuli were similar (M-AIR, *top panel*, $P = 0.279$ and $P = 0.357$ for peak amplitude and τ_{DEC}, respectively).

Effects of blockade of medullary PPs were assessed by monitoring peak amplitude and τ_{DEC} of M-AIRs provoked by the test stimulus of each pair before and after a single injection of Glu antagonists. Under this condition, injections of blockers

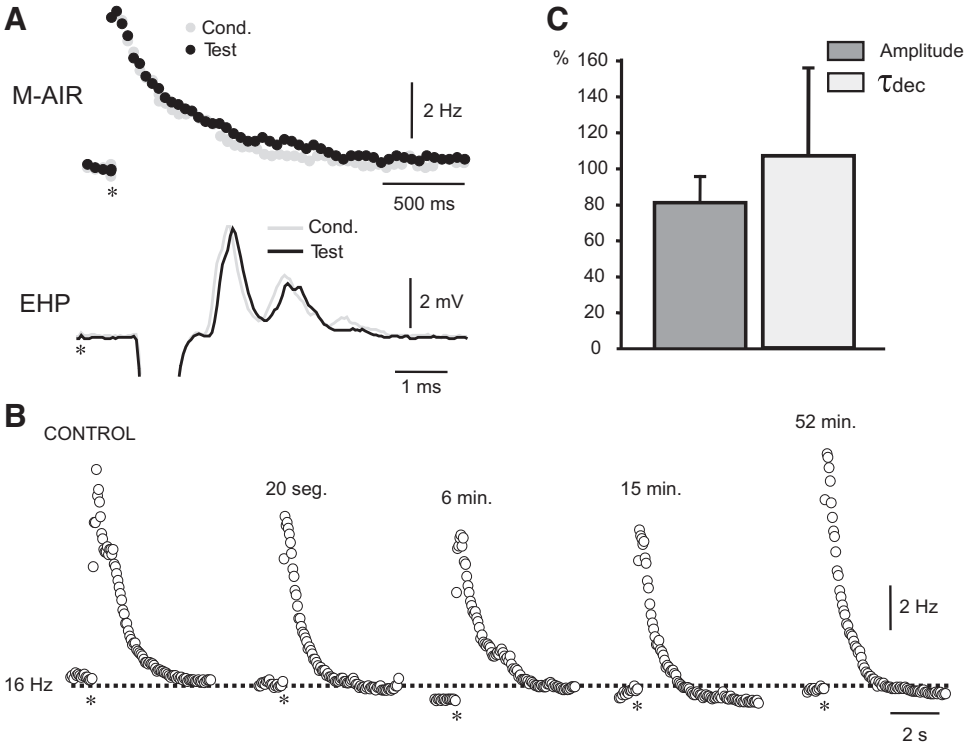

FIG. 6. Amplitude of M-AIR results critically from activation of medullary PPs. *A*: paired M-cell activation at 8 s delay does not modify M-AIR but reduces synaptic efficacy at M-cell–associated circuits. *Top* (M-AIR): plots of EOD frequency vs. time of M-AIRs elicited by conditioning (● Cond.) and test (●, Test) stimuli of a pair. *Bottom* (EHP): superimposed field potential recordings in the vicinity of the left M-cell axon cap in response to the same pair of stimuli (gray line, Cond.; black line, Test). Note that paired M-cell axon activation provoked an increase in latency and a reduction in amplitude of late positive components of evoked field potentials. Antidromic M-cell spikes of ~8 mV were truncated. *B*: plots of EOD frequency vs. time of M-AIRs obtained before (CONTROL) and after (intervals indicated over each plot) a bilateral pressure ejection of Glu antagonists (AP5 500 μM and CNQX 500 μM in NaCl 154 mM, 25 psi, 300 ms) at medullary PPs. In *A* and *B*, the moment of M-cell axon activation is indicated by an asterisk. In *B*, dashed line shows basal EOD frequency indicated by the number at *left*. *C*: summary data (mean ± SD, $n = 43$ injections) of effects of medullary PPs blockade on the amplitude (dark gray bar) and decay time constant (τ_{DEC}, light gray bar) of M-AIRs evoked by test stimulus of each pair (8 s delay), plotted as percentages of their respective control values.

were effective in 43 of 48 injections (89.6%). An example of Glu antagonist–induced changes in M-AIR is shown in Fig. 6*B,* wherein the injection of blockers at a site 1,000 μm rostral to the PMn produced a reduction of peak amplitude of M-AIR to 77% of control (6 min after injection), an effect that vanished 52 min after injection. A summary of results (21 animals, 43 injections) is shown in Fig. 6*C*. Compared with control conditions, there was a reduction in the M-AIR peak amplitude to a mean value of 80.2 ± 15.1% ($P < 0.0001$); this reduction was observed after a mean interval of 11 min (range, 5–16 min), with a mean recovery time of 98.5 min (range, 40–170 min). In contrast, although reduction of M-AIR peak amplitude was often accompanied by a decrease in total duration, τ_{DEC} was not affected by medullary PPs blockade (106.4 ± 47.8%, $P = 0.58$).

Injections of Glu antagonist within the PPs at the caudal medulla that produced a transient reduction of M-AIR peak amplitude did not affect the response to Glu (10 mM) on EOD rate when applied near PM-cells at the PMn ($n = 3$, Supplemental Fig. S1).[1]

DISCUSSION

PPs in G. omarorum

This study provides the first description of PPs in *G. omarorum*. After application of the tracer at the PMn, retrograde-labeled cells distributed unevenly within a bilateral rostrocaudal column that extended from the diencephalon to the caudal medulla (Fig. 3). Marked neurons tended to aggregate near the CP in the thalamus and in the octavolateral area. Although more dispersed, a third group of labeled cells appeared in the caudal medulla between the M-cells and the rostral pole of the PMn. In addition, we found that Glu applied in these three areas (diencephalon, octavolateral, and caudal medulla) produced short-latency and transient increases in EOD rate (Fig. 4).

These results showed a distribution of PPs in *G. omarorum* that contrasts with data previously reported vis a vis the distribution of PPs in other gymnotiform fish (Heiligenberg et al. 1981; Kawasaki and Heiligenberg 1989; Kawasaki et al. 1988; Keller et al. 1990, 1991; Kennedy and Heiligenberg 1994). Prepacemaker neurons have been grouped in two bilateral aggregates located in the diencephalon and mesencephalon, which have been designated as the diencephalic (PPn) and the sublemniscal (sPPn) prepacemaker nuclei, respectively.

It seems unlikely that the neuronal labeling at unforeseen medullary PPs may have resulted from nonspecific labeling caused by extensive diffusion of tracer from the site of injection. As can be concluded from the close examination of the injection site within the PMn in our tracing experiments, the tracer was exclusively present within PM-cells (see Fig. 1*C* and RESULTS). Moreover, modulations of EOD rate produced by activation of neuronal groups located in the octavolateral area and the caudal medulla (Fig. 4, *B* and *C*) strongly suggest that these neurons are also functionally prepacemaker cells. The small number of labeled cells per animal and the fact that they were distant from the site of injection of the marker further confirm the notion that the biocytin-labeled neurons innervate the PMn. However, nonspecific labeling, if any, cannot be completely ruled out because of uptake of biocytin by some damaged fibers of the medial longitudinal fasciculus during the descent of the pipette containing the tracer solution to the PMn (see Fig. 1*B*). It has been proposed that physical damage is necessary for biocytin uptake by fibers of passage during tracing experiments (Vercelli et al. 2000).

PPs: The linkage between the electrosensory system and M-cell–related networks

PPs have been first described as the neural interface between sensory systems and the electrogenic component of the active electroreceptive neural system responsible for the organization of sensory-evoked EOD modulations (Giassi et al. 2007; Heiligenberg et al. 1981; Kawasaki et al. 1988; Keller et al. 1990; Metzner 1999). However, tract-tracing techniques (see, for example, Wong 1997; for a review, see Zupanc 2002) also showed that a wide variety of nonsensory central structures project to PPs. Consequently, PPs might also integrate inputs arising from nonsensory related areas to promote specific EOD modulations. In this study, we showed that, in addition to their role in the organization of sensory-evoked EOD modulations, PPs in gymnotiform fish may also participate in the organization of the M-AIR, a modulation of the electrosensory system triggered by a neural signal that takes origin in the M-cell, a central component of the motor neural system responsible for escape.

Based on the latency of M-cell–initiated synaptic actions at PM cells (Falconi et al. 1997) and the characteristics of M-cell–evoked field potential near the PMn (Curti et al. 2006), we have previously postulated that a group of as yet unidentified interneurons (Int. in Fig. 7*B*), similar to cranial relay neurons (CRN) described in goldfish, is interposed between the M-cell axons and PPs. Moreover, location of prepacemaker neurons far away from M-cell axons even for medullary PPs (>300 μm, this study) together with the fact that M-cell axon in *Gymnotus omarorum* emits few short processes (Trujillo-Cenóz and Bertolotto 1990), probably as those described in goldfish and other teleosts (Funch et al. 1984; Ritter et al. 2001), also suggest that connections between M-cell and PPs neurons are mediated by a group of specialized interneurons.

Results from lesion and local transient blockade experiments (Figs. 5 and 6) indicate that PPs involved in M-AIR are functionally segregated. Whereas diencephalic PPs critically determine the duration of the M-AIR, its peak amplitude relies on the activation of the more caudal PPs. An estimation of their relative contribution to M-AIR is shown in Fig. 7*A*. By point-by-point subtraction of a control M-AIR (top trace) and a remnant M-AIR after brain stem section (medullary component, middle trace), the contribution of diencephalic PPs (bottom trace) can be estimated. The medullary component is relatively brief and mainly responsible for the abrupt increase in rate and peak magnitude of the response, whereas the diencephalic component is slow, long-lasting, and more relevant during the late part of the M-AIR.

A wealth of evidence derived from the study of PPs in several gymnotiform fish strongly suggests that the functional specialization of discrete PPs regions is probable a general organizing principle of prepacemaker networks (Kawasaki and

[1] The online version of this article contains supplemental data.

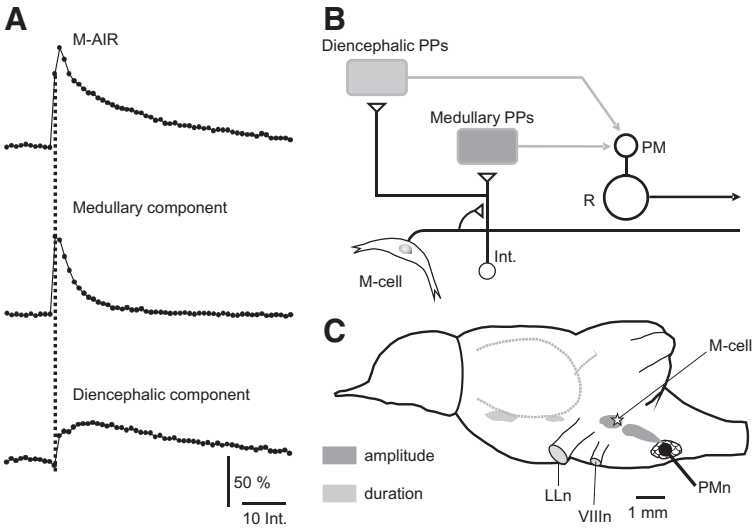

FIG. 7. Diencephalic and medullary PPs involved in M-AIR are functionally segregated. *A*: plots of EOD frequency (normalized) vs. interval number of a representative M-AIR (M-AIR, *top plot*), the remnant M-AIR after a complete brain stem section at the level indicated in Fig. 5*A* (medullary component, *middle plot*), and the result of a point-by-point substraction of these 2 responses (diencephalic component, *bottom plot*). The vertical dotted line indicating the 1st interval of the control response is included to facilitate comparison between plots. *B*: diagram of the putative neural circuit that mediates M-AIR. The M-cell probably innervates an as yet unidentified group of interneurons (Int.), which in turn innervates diencephalic and medullary PPs. Pacemaker cells, receiving PPs innervation, and R-cells are also depicted. Diencephalic and medullary PPs exhibited different dashing pattern (key included in *C*) to show their dissimilar functional role in the organization of M-AIR. *C*: schematic drawing of a lateral view of the brain of *G. omarorum* showing, more realistically, the distribution and functional specialization of PPs involved in M-AIR. As in Fig. 5*A*, several anatomical details were included in the scheme for reference. Key of their role in the organization of M-AIR is shown in the *bottom left*.

Heiligenberg 1990; Kennedy and Heiligenberg 1994; see also Caputi et al. 2005). Moreover, each subdivision seems to be activated independently during a definite behavioral display. However, our data suggest that the motor command arising from the M-cell may result in simultaneous activation of PPs with apparently disparate functional specialization (Fig. 7, *B* and *C*). Massive recruitment of different PPs during M-AIR overriding a more precise and probably behavior-related pattern of PPs activation indicate a well-shown general functional characteristic of M-cell dependent circuits (Eaton et al. 2001; Korn and Faber 2005). Convincing physiological evidence indicates that there is a priority of the escape reaction over other motor behaviors (Svoboda and Fetcho 1996) because of a high safety factor at all connections downstream from the M-cell (Fetcho 1991).

M-AIR: The modulation of an active sensory system by a motor-derived signal

A wealth of evidence obtained from both vertebrate and invertebrate experimental models indicates that most neural designs underlying high-level motor–sensory interactions, although with a wide variety of functions, involve the modulation of sensory processing by motor-derived neural signals (Crapse and Sommer 2008; Poulet and Hedwig 2006). However, as reported in the last few years (Friedman et al. 2006; Wilson and Moss 2004), high-level motor–sensory interactions may also include neural designs allowing the modulation of the motor component of the active sensing systems by collaterals of central motor commands, leading to adaptive changes of sensory sampling during definite behavioral contexts (Nelson

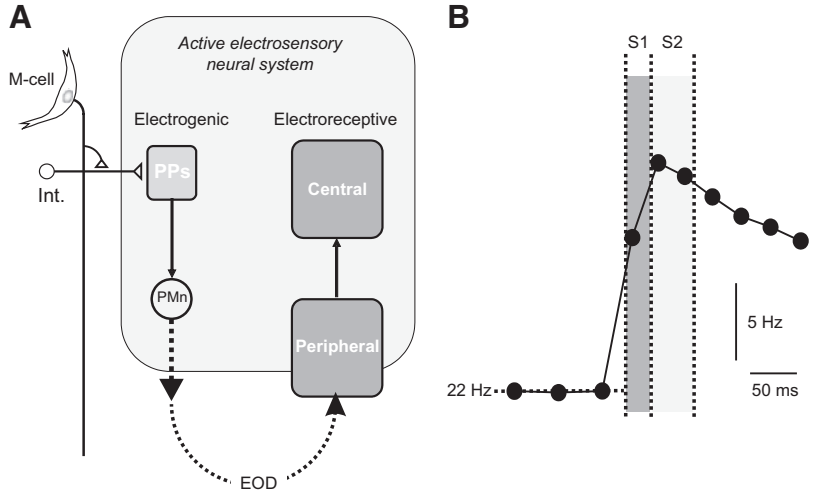

FIG. 8. Proposed neural basis and possible functional implications of the modulation of the electrosensory system by an M-cell–derived signal. *A*: diagram of the neural pathway connecting the M-cell and the active electrosensory neural system. For the sake of simplicity, this system is represented by blocks connected by arrows showing the PPs and the PMn as parts of its electrogenic component and central and peripheral structures of its electroreceptive component. A reafferent EOD pathway linking both components at the periphery is also shown. The M-cell–derived signal modulates the electrogenic component of the active electrosensory system via a group of interneurons (Int.) innervating the PPs. *B*: schematics of the temporal correlation of M-AIR and the 2 phases of escape response in teleosts. Plot of EOD frequency vs. time of a representative M-AIR in which the approximate timing of the initial components of escape response (according to Eaton et al. 2001) is represented by the dark and light gray rectangles delimited by vertical dotted lines. The dark gray region indicate the stage I (S1) of the response that begins about 12 ms after M-cell activation, lasts for 25 ms, and is considered an evasive, relatively stereotyped response that is highly dependent on M-cell activation. The stage 2 (S2) that immediately follows the 1st stage is shown by the light gray region. This stage lasts for ~45 ms, is propulsive, is variable, and most likely results from activation of a group of M-cell–like reticulospinal neurons. Note that the start of S2 approximately coincides with the peak of M-AIR.

and MacIver 2006). In certain bats, for example, during prey capture, later phases of behavioral displays are accompanied by an increase in the emission rate of echolocating signals that may help fine control of its flight behavior before contact (Wilson and Moss 2004). Similar modulations of active sensing systems during certain motor behaviors have also been reported in rats. During exploration, whisking behavior (Friedman et al. 2006; Grant et al. 2009), a widely used model of active touch in rodents, as well as the frequency of sniffing (Verhagen et al. 2007), display specific changes likely involved in the boosting of the amount of useful sensory information with probable perceptual consequences.

This study shed light on the neural basis of an example of this kind of motor–sensory interaction in a gymnotiform fish. Our data indicate that the modulation of the electrogenic component of the active electrosensory system by a central motor command involves a relatively simple neural pathway that includes the activation of specialized brain stem neurons (PPs) by the command neuron for escape (M-cells) through a population of as yet unidentified interneurons (Fig. 8*A*). This neural design is apparently well suited to increase sensory sampling in close temporal relationship with the motor display. However, what could be the functional role of an enhancement of electrosensory sampling precisely timed with motor escape? A possible answer for this question emerges from the analysis of the correlation of the two concurrent functional consequences of M-cell activation: the M-AIR and the motor escape (Fig. 8*B*). In most teleosts, the initial component of the escape response (known as the C-start) consists of two successive phases (Eaton et al. 2001). The first phase (stage 1) consists of a highly stereotyped C-bend of the fish body triggered by activation of M-cells. This phase is likely an evasive response that is achieved in ~30 ms. The second phase (stage 2) consists in a propulsive turn of the body that begins at the end of the C-bend and most likely results from activation of a population of M-cell–like reticulospinal cells. Several parameters of this motor act, including the escape trajectory, result from integration of multimodal sensory information acquired presumably at the end of the first phase. Although a rigorous kinematic study of escape has not yet been performed in gymnotiforms, preliminary behavioral observations in *Gymnotus omarorum* using video recordings suggest that kinematics of escape responses in this species is similar that of goldfish (Borde et al. 2004). As shown in Fig. 8*B*, the start of stage 2 likely occurs during the peak of M-AIR, allowing the fish to rapidly update electrosensory information about environment just before the execution of the propulsive phase of escape. The population of M-cell–like reticulospinal cells may process this information for selecting the escape trajectory. Interestingly, experimental evidence obtained in a related genus strongly suggests that escape responses may be influenced by electrosensory clues (Canfield and Rose 1993).

In conclusion, our study contributes to an understanding of the neural basis of a high-level motor–sensory interaction strategy in a vertebrate model characterized by the modulation of the motor component of an active sensory system triggered by a motor command. In *G. omarorum*, this modulation likely represents an enhancement of the fish sampling capability of the environment during M-cell–initiated motor behaviors that provides crucial electrosensory information for an adequate selection of the escape trajectory.

ACKNOWLEDGMENTS

We thank C. Rivero, A. Falconi, and S. Curti, although during different periods, for assistance in some pilot lesion and pharmacological experiments. We thank Drs. Washington Buño, Omar Macadar, and Jack Yamuy for valuable suggestions regarding the manuscript and assistance in English editing. We also thank Dr. José Antonio Muñoz Cueto for expert advice in the interpretation of results from labeling experiments.

GRANTS

This work was partially supported by Banco Interamericano de Desarrollo-Consejo Nacional de Investigación Científica y Tecnológica Grant 353, Programa de Desarrollo Tecnológico Grant S/C/IF/54/090, a Comisión Sectorial de Investigación Científica - Universidad de la República grant, and Programa de Desarrollo de las Ciencias Básicas - Uruguay.

DISCLOSURES

No conflicts of interest, financial or otherwise, are declared by the authors.

REFERENCES

Barrio LC, Caputi A, Crispino L, Buño W. Electric organ discharge frequency modulation evoked by water vibration in *Gymnotus carapo*. *Comp Biochem Physiol* 100A: 555–562, 1991.

Bell CC. Sensory coding and corollary discharge effects in mormyrid electric fish. *J Exp Biol* 146: 229–253, 1989.

Borde M, Curti S, Comas V, Rivero C. Central modulation of a sensory system by a motor command. One intention with two results. *Rev Neurol* 38: 253–260, 2004.

Borde M, Pereda AE, Morales FR. Electrophysiological characteristics of the Mauthner cell of the weakly electric fish *Gymnotus carapo*. *Brain Res* 567: 145–148, 1991.

Canfield JG, Rose GJ. Electrosensory modulation of escape responses. *J Comp Physiol [A]* 173: 463–474, 1993.

Caputi AA. Contributions of electric fish to the understanding sensory processing by reafferent systems. *J Physiol Paris* 98: 81–97, 2004.

Caputi AA, Carlson B, Macadar O. Electric organs and their control. In: *Electroreception*, edited by Bullock TH, Hopkins CD, Popper A, Fay R. New York: Springer, 2005, p. 410–451.

Charpier S, Behrends JC, Chang YT, Sur C, Korn H. Synchronous bursting in a subset of interneurons inhibitory to the goldfish Mauthner cell: synaptic mediation and plasticity. *J Neurophysiol* 72: 531–541, 1994.

Crapse TB, Sommer MA. Corollary discharge across the animal kingdom. *Nat Rev Neurosci* 9: 587–600, 2008.

Curti S, Comas V, Rivero C, Borde M. Analysis of behavior-related excitatory inputs to a central pacemaker nucleus in a weakly electric fish. *Neuroscience* 140: 491–504, 2006.

Curti S, Falconi A, Morales FR, Borde M. Mauthner cell-initiated electromotor behavior is mediated via NMDA and metabotropic glutamatergic receptors on medullary pacemaker neurons in a gymnotid fish. *J Neurosci* 19: 9133–9140, 1999.

Eaton RC, Lee RK, Foreman MB. The Mauthner cell and other identified neurons of the hindbrain escape network of fish. *Prog Neurobiol* 63: 467–485, 2001.

Faber DS, Fetcho JR, Korn H. Neuronal networks underlying the escape response in goldfish. *Ann NY Acad Sci USA* 563: 11–33, 1989.

Faber DS, Korn H. Electrophysiology of the Mauthner cell: basic properties, synaptic mechanisms, and associated networks. In: *Neurobiology of the Mauthner Cell*, edited by Faber DS, Korn H. New York: Raven, 1978, p. 47–126.

Falconi A, Borde M, Hernandez-Cruz A, Morales FR. Mauthner cell-initiated abrupt increase of the electric organ discharge in the electric fish *Gymnotus carapo*. *J Comp Physiol [A]* 176: 679–689, 1995.

Falconi A, Lorenzo D, Curti S, Morales FR, Borde M. Mauthner cell-evoked synaptic actions on pacemaker medullary neurons of a weakly electric fish. *J Comp Physiol [A]* 181: 143–151, 1997.

Fetcho JR. Spinal network of the Mauthner cell. *Brain Behav Evol* 37: 298–316, 1991.

Friedman WA, Jones LM, Cramer NP, Kwegyir-Afful EE, Zeigler HP, Keller A. Anticipatory activity of motor cortex in relation to rhythmic whisking. *J Neurophysiol* 95: 1274–1277, 2006.

Funch PG, Wood MR, Faber DS. Localization of active sites along the myelinated goldfish Mauthner axon: morphological and pharmacological evidence for saltatory conduction. *J Neurosci* 4: 2397–2409, 1984.

Furshpan EJ, Furukawa TJ. Intracellular and extracellular responses of the several regions of the Mauthner cell of the goldfish. *J Neurophysiol* 25: 732–771, 1962.

Furukawa TJ, Furshpan EJ. Two inhibitory mechanisms in the Mauthner neurons of goldfish. *J Neurophysiol* 26: 140–176, 1963.

Giassi AC, Corrêa SA, Hoffmann A. Fiber connections of the diencephalic nucleus tuberis anterior in the weakly electric fish, *Gymnotus cf. carapo*: an in vivo tract-tracing study. *J Comp Neurol* 503: 655–667, 2007.

Grant RA, Mitchinson B, Fox CW, Prescott TJ. Active touch sensing in the rat: anticipatory and regulatory control of whisker movements during surface exploration. *J Neurophysiol* 101: 862–874, 2009.

Heiligenberg W, Finger T, Matsubara J, Carr C. Input to the medullary pacemaker nucleus in the weakly electric fish, *Eigenmannia* (Sternopygidae, gymnotiformes). *Brain Res* 211: 418–423, 1981.

Horikawa K, Armstrong WE. A versatile means of intracellular labeling: injection of biocytin and its detection with avidin conjugates. *J Neurosci Methods* 25: 1–11, 1988.

Juranek J, Metzner W. Segregation of behavior-specific synaptic inputs to a vertebrate neuronal oscillator. *J Neurosci* 18: 9010–9019, 1998.

Kawasaki M, Heiligenberg W. Distinct mechanisms of modulation in a neuronal oscillator generate different social signals in the electric fish, *Hypopomus*. *J Comp Physiol [A]* 165: 731–741, 1989.

Kawasaki M, Heiligenberg W. Different classes of glutamate receptors and GABA mediate distinct modulations of a neuronal oscillator, the medullary pacemaker of a gymnotiform electric fish. *J Neurosci* 10: 3896–3904, 1990.

Kawasaki M, Maler L, Rose GJ, Heiligenberg W. Anatomical and functional organization of the prepacemaker nucleus in gymnotiform electric fish: the accommodation of two behaviors in one nucleus. *J Comp Neurol* 276: 113–131, 1988.

Keller CH, Kawasaki M, Heiligenberg W. The control of pacemaker modulations for social communication in the weakly electric fish *Sternopygus*. *J Comp Physiol [A]* 169: 441–450, 1991.

Keller CH, Maler L, Heiligenberg W. Structural and functional organization of a diencephalic sensory-motor interface in the gymnotiform fish, *Eigenmannia*. *J Comp Neurol* 293: 347–376, 1990.

Kennedy G, Heiligenberg W. Ultrastructural evidence of GABA-ergic inhibition and glutamatergic excitation in the pacemaker nucleus of the gymnotiform electric fish, *Hypopomus*. *J Comp Physiol [A]* 174: 267–280, 1994.

Korn H, Faber DS. The Mauthner cell half a century later: a neurobiological model for decision-making? *Neuron* 47: 13–28, 2005.

Lissman HW, Machin KE. The mechanism of object location in *Gymnarchus niloticus* and similar fish. *J Exp Biol* 35: 451–486, 1958.

Lorenzo D, Silva AC, Borde M, Macadar O. Electrogeneration in South American weakly electric fish. In: *Sensory Biology of Jawed Fishes: New Insights*, edited by Kapoor BG, Hara TJ. New Delhi: Oxford and IBH Publishing, 2001, p. 121–159.

Maler L, Sas E, Johnston S, Ellis W. An atlas of the electric fish *Apteronotus leptorhynchus*. *J Chem Neuroanat* 4: 1–38, 1991.

McCloskey DJ. Corollary discharges: motor commands and perception. In: *Handbook of Physiology. Nervous System II*, edited by Brookhart JM, Mountcastle VB, Brooks VB, Geiger SR. Bethesda, MD: American Physiological Society, 1981, 1415–1447.

Metzner W. Neural circuitry for communication and jamming avoidance in gymnotiform electric fish. *J Exp Biol* 202: 1365–1375, 1999.

Morales FR, Falconi A, Hernandez-Cruz A, Borde M. Abrupt increase in the rate of the electric organ discharge initiated by the Mauthner cell in *Gymnotus carapo*. *J Comp Physiol [A]* 173: 751, 1993.

Nelson ME, MacIver MA. Sensory acquisition in active sensing systems. *J Comp Physiol [A]* 192: 573–586, 2006.

Poulet JF, Hedwig B. The cellular basis of a corollary discharge. *Science* 27: 518–522, 2006.

Richer-de-Forges M, Crampton WGR, Albert JS. A new species of Gymnotus (Gymnotiformes, Gymnotidae) from Uruguay: description of a model species in neurophysiological research. *Copeia* 3: 538–544, 2009.

Ritter DA, Bhatt DH, Fetcho JR. In vivo imaging of zebrafish reveals differences in the spinal networks for escape and swimming movements. *J Neurosci* 21: 8956–8965, 2001.

Santana UJ, Roque-da-Silva AC, Duarte TT, Corrêa SA. Interference with the GABAergic system in the dorsolateral telencephalon and modulation of the electric organ discharge frequency in the weakly electric fish. *Gymnotus carapo. J Comp Physiol [A]* 187: 925–933, 2001.

Sawtell NB, Williams A, Bell CC. From sparks to spikes: information processing in the electrosensory systems of fish. *Curr Opin Neurobiol* 15: 437–443, 2005.

Sommer MA, Wurtz RH. Brain circuits for the internal monitoring of movements. *Annu Rev Neurosci* 31: 317–338, 2008.

Sperry RW. Neural basis of the spontaneous optokinetic response. *J Comp Physiol Psychol* 43: 482–489, 1950.

Svoboda KR, Fetcho JR. Interactions between the neural networks for escape and swimming in goldfish. *J Neurosci* 16: 843–852, 1996.

Trujillo-Cenóz O, Bertolotto C. Mauthner cells in the medulla of the weakly electric fish *Gymnotus carapo. Experientia* 46: 441–443, 1990.

Vercelli A, Repici M, Garbossa D, Grimaldi A. Recent techniques for tracing pathways in the central nervous system of developing and adult mammals. *Brain Res Bull* 51: 11–28, 2000.

Verhagen JV, Wesson DW, Netoff TI, White JA, Wachowiak M. Sniffing controls an adaptive filter of sensory input to the olfactory bulb. *Nat Neurosci* 10: 631–639, 2007.

von Holst E, Mittelstaedt H. The reafference principle. Interactions between the central nervous system and the periphery. *Naturwissenchaften* 37: 464–476, 1950.

Waldeck RF, Pereda A, Faber DS. Properties and plasticity of paired-pulse depression at a central synapse. *J Neurosci* 20: 5312–5320, 2000.

Webb B. Neural mechanisms for prediction: do insects have forward models? *Trends Neurosci* 27: 278–282, 2004.

Wilson WW, Moss CF. Sensory-motor behavior of free-flying FM bats during target capture. In: *Advances in the Study of Echolocation in Bats and Dolphins*, edited by Thomas JA, Moss CF, Vater M. Chicago, IL: Chicago University Press, 2004, p. 22–27.

Wong CJ. Afferent and efferent connections of the diencephalic prepacemaker nucleus in the weakly electric fish, *Eigenmannia virescens*: interactions between the electromotor system and the neuroendocrine axis. *J Comp Neurol* 383: 18–41, 1997.

Zupanc GK. From oscillators to modulators: behavioral and neural control of modulations of the electric organ discharge in the gymnotiform fish, *Apteronotus leptorhynchus*. *J Physiol Paris* 96: 459–472, 2002.